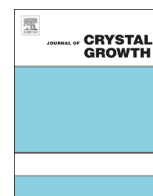




ELSEVIER

Contents lists available at ScienceDirect

Journal of Crystal Growth

journal homepage: [www.elsevier.com/locate/jcrysgro](http://www.elsevier.com/locate/jcrysgro)

# Effect of ultrasonic melt treatment on the refinement of primary Al<sub>3</sub>Ti intermetallic in an Al–0.4Ti alloy



Feng Wang<sup>a,\*</sup>, Dmitry Eskin<sup>a,b</sup>, Thomas Connolley<sup>c</sup>, Jiawei Mi<sup>d</sup>

<sup>a</sup> Brunel Centre for Advanced Solidification Technology, Brunel University London, Uxbridge, London UB8 3PH, UK

<sup>b</sup> Tomsk State University, Tomsk 634050, Russia

<sup>c</sup> Diamond Light Source Ltd, Harwell Science & Innovation Campus, Didcot OX11 0DE, UK

<sup>d</sup> School of Engineering, University of Hull, Hull, East Yorkshire HU6 7RX, UK

## ARTICLE INFO

### Article history:

Received 15 October 2015

Received in revised form

3 November 2015

Accepted 7 November 2015

Communicated by Christopher Gourlay

Available online 4 December 2015

### Keywords:

A1. Crystal morphology

A1. Solidification

A1. Ultrasonic treatment

A2. Growth from melt

B1. Alloys

B1. Intermetallics

## ABSTRACT

High intensity ultrasonic melt treatment was applied to an Al–0.4 wt% Ti alloy over three selected temperature ranges: 810 to 770 °C (above liquidus), 770 to 730 °C (across liquidus), and 730 to 690 °C (below liquidus). The size and morphology of the primary Al<sub>3</sub>Ti intermetallic particles were studied by scanning electron microscopy. It was found that the primary Al<sub>3</sub>Ti intermetallics were refined as a result of ultrasonication over all three temperature ranges and their morphology changed from typical large dendritic plates to small compact tablets. Quenching experiments before and after the ultrasonication were also carried out to capture the high-temperature stage of intermetallic formation. Based on the size and morphology observations, the mechanisms for the refinement of primary Al<sub>3</sub>Ti intermetallics at different solidification stages are discussed.

© 2015 The Authors. Published by Elsevier B.V. This is an open access article under the CC BY license (<http://creativecommons.org/licenses/by/4.0/>).

## 1. Introduction

The application of high-intensity ultrasound to the processing of liquid or semi-liquid metal alloys during casting is attractive to metallurgists in academia and industry because it provides a cost-effective and sustainable method for the improvement of the quality of cast products [1,2]. It has been demonstrated that high-power ultrasonic vibrations can result in significant beneficial changes in microstructure including the refinement of dendritic grains, primary intermetallic particles and/or eutectic phases, increasing structural homogeneity and reducing chemical segregation [1,3,4]. In addition, ultrasonic melt treatment (UST) can be also used for melt degassing, filtration and fabrication of metal matrix composites [1,5,6].

Recently, the refinement of primary intermetallic particles has attracted increasing attention in research because it can considerably improve mechanical properties, corrosion resistance, wear resistance, thermal stability and formability of the solidified alloys [1,3,7,8]. Furthermore, some of the primary intermetallic compounds [4,9,10] are known to have strong potency as nucleation sites for new grains. Hence, refinement of these primary

intermetallics can promote further grain refinement for the alloy matrix and therefore increase the mechanical properties of the castings.

The effectiveness of UST is affected by many factors as reported in the literature [1,4,8,11,12], for example, the amplitude and frequency of ultrasound, treatment temperature and duration, and the solidification conditions, i.e. cooling rate, alloy composition and impurity level. Among all these factors, the treatment temperature range [4,8,13] plays an important role in determining the efficiency of UST because alloy melt viscosity, which is mainly controlled by melt temperature [1,2], is one of the major factors in determining the efficiency of UST when it is applied in the fully liquid state. More importantly, at different temperature ranges and dependent on the alloy systems, solidification occurs and proceeds with different characteristic stages, e.g. initial nucleation stage, following growth stage, etc. UST in different temperature ranges may involve different mechanisms which ultimately control the efficiency of UST in modifying microstructure.

This paper presents a recent study on UST of an Al–0.4% Ti alloy over different temperature ranges, with a focus on the formation of primary Al<sub>3</sub>Ti intermetallic compounds. This work was done to understand and clarify the mechanisms and effectiveness of UST on refining primary intermetallic at different solidification stages. (All the chemical compositions throughout the paper are in weight percent unless otherwise stated)

\* Corresponding author.

E-mail address: [feng.wang@brunel.ac.uk](mailto:feng.wang@brunel.ac.uk) (F. Wang).

## 2. Experimental

### 2.1. Materials and apparatus

The Al–0.4% Ti alloy was prepared from high-purity commercial aluminium (99.97%) and Al–10% Ti master alloy. The liquidus temperature of primary  $\text{Al}_3\text{Ti}$  in the Al–0.4%Ti alloy was calculated to be 768 °C using the TCAL3 database of the ThermoCalc software [14].

The ultrasonic system consists of a 5-kW ultrasonic generator, a magnetostrictive transducer (RELTEC) with water cooling system and an ultrasonic sonotrode made of niobium. Ultrasonic treatment was performed at 4-kW power with the frequency of 17.5 kHz and the corresponding peak-to-peak amplitude 40  $\mu\text{m}$  as measured by a contactless vibrometer in air.

### 2.2. Casting and ultrasonic treatment procedure

Pure Al (~500 g for each experiment) was melted in a clay-bonded graphite crucible inside an electrical resistance furnace and heated up to  $880 \pm 3$  °C, at which point the master alloy was added. After 30 min isothermal holding following the addition of master alloy, the crucible with melt was transferred to a platform where the ultrasound was applied to the melt. The melt was cooled in air, and its temperature was monitored by a K-type thermocouple positioned at approximately half the radius away from the wall of crucible. When the melt temperature decreased to the target temperature, the sonotrode was immersed 15 mm below the top surface of the melt. To avoid the chill effect of a cold sonotrode, the sonotrode was turned on and preheated inside a crucible containing 2.5 kg pure Al melt (~800 °C) for about 30 s before it was inserted into the melt to be treated. This operation avoided any noticeable temperature drop when the sonotrode was immersed into the melt, and therefore the cooling rate did not change much. In addition, an experiment without UST was also carried out by immersing the sonotrode (without vibration) into the melt at the same temperature as the experiment with UST. The sonotrode was not lifted up from the melt until the melt temperature reached the designed termination temperature. The melt together with the crucible was then left on the platform to solidify in air to room temperature. The overall cooling rate measured by thermocouple was ~0.8 °C/s. The chemical compositions of the alloys was analysed by inductively coupled plasma-atomic emission spectroscopy (ICP-AES) and the averaged values are listed in Table 1. Three temperature ranges were selected, corresponding to three different solidification stages: 810 to 770 °C (fully liquid state), 770 to 730 °C (the nucleation stage of primary  $\text{Al}_3\text{Ti}$ ), and 730 to 690 °C (the growth stage of primary  $\text{Al}_3\text{Ti}$ ).

In order to capture the formation of primary  $\text{Al}_3\text{Ti}$  intermetallics, quenched samples were obtained at temperatures when the sonotrode was inserted into and lifted up from the melt for each experiment. This was done by sucking the alloy melt into a quartz tube using a syringe followed by quenching the tube in water. The inner diameter of the quartz tube was 3 mm with a wall thickness of 1 mm.

### 2.3. Sample preparation and examination

The solidified ingots were longitudinally sectioned along the centre symmetrical axis and specimens were prepared from the

central bottom part as shown in the schematic diagram (Fig. 1) because most of the primary  $\text{Al}_3\text{Ti}$  particles settled down to the bottom due to the larger density of  $\text{Al}_3\text{Ti}$  and slow cooling rate. The specimens from the ingot and the quenched tube were then mechanically ground and polished for scanning electron microscopy (SEM, ZEISS SUPRA 35VP). Energy dispersive X-ray spectroscopy was used to determine the composition of the particles observed in the samples. In order to display the 3D morphology of the primary  $\text{Al}_3\text{Ti}$  intermetallic, the samples with and without UST were deeply etched by a 15% NaOH water solution for about 2 h. The deeply etched samples were then also examined by SEM.

## 3. Results and discussion

### 3.1. Effect of UST on the size of primary $\text{Al}_3\text{Ti}$ intermetallic particles

Fig. 2 shows the typical SEM backscatter electron (BSE) images of the primary  $\text{Al}_3\text{Ti}$  intermetallic particles from the ingot specimens with and without UST. Apparently, UST for all three cases showed the effect on the refinement of primary  $\text{Al}_3\text{Ti}$  particles. It is noteworthy that, in the current work, the application of UST in the liquid state (from 810 to 770 °C while the liquidus temperature of  $\text{Al}_3\text{Ti}$  is 768 °C) produced significant refining effect on the primary  $\text{Al}_3\text{Ti}$  intermetallic as presented in Fig. 1(b). In addition, both large and small  $\text{Al}_3\text{Ti}$  particles are observed in the sample after UST from 730 to 690 °C as shown in Fig. 1(d).

The measured size distributions of the primary  $\text{Al}_3\text{Ti}$  particles in the samples without UST (but in the presence of an idle sonotrode) were presented in Fig. 3(a)–(c) and revealed that the majority of primary intermetallics are in the range 50–200  $\mu\text{m}$ , while some of them even grew to ~500  $\mu\text{m}$ . These are mainly because of the large solidification range for the primary intermetallic and slow cooling rate to allow the particles to grow sufficiently. When the UST was applied from 810 to 770 °C, almost all particles were reduced to below 20  $\mu\text{m}$  with the majority in the range of 3–8  $\mu\text{m}$  as illustrated in Fig. 3(a). From Fig. 3(b) we can see that UST from 770 to 730 °C also considerably refined the primary intermetallics to 2–60  $\mu\text{m}$ , and the majority of the particles lies between 8 and 15  $\mu\text{m}$ . Fig. 3(c) illustrates the size

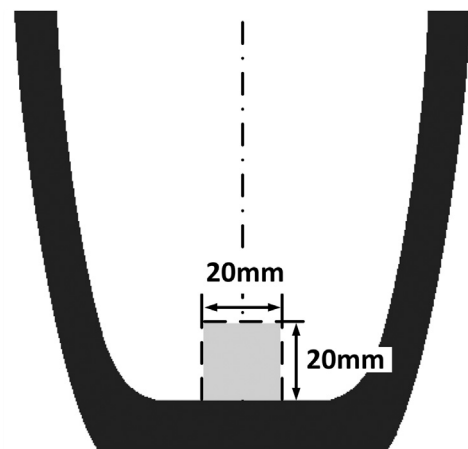
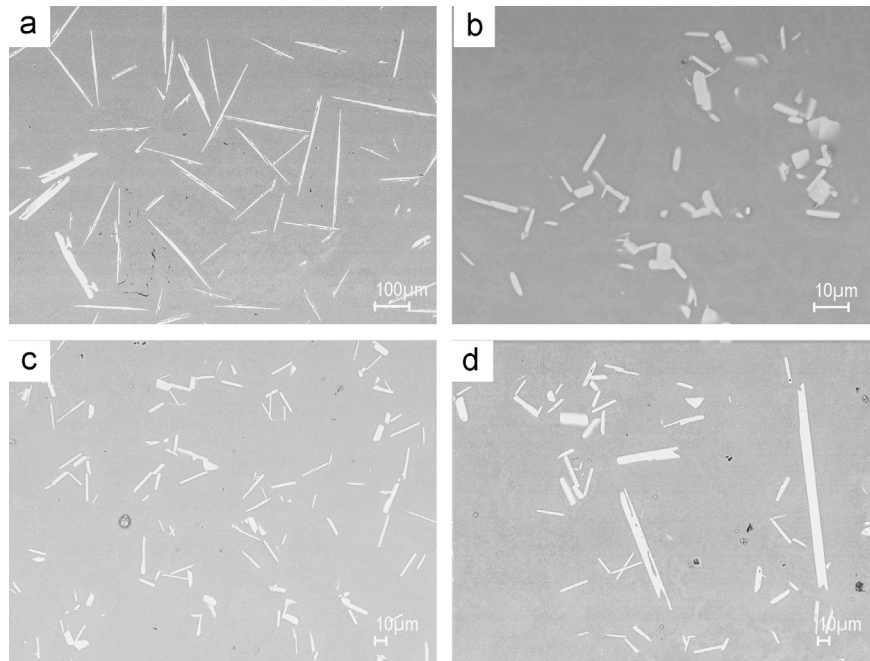


Fig. 1. Schematic diagram of the relative position of microstructure specimen.

Table 1

The averaged chemical compositions of the Al–0.4% Ti alloys.

Al	Ti	B	Si	Fe	Cu	Mn	Mg	Zn
Bal.	$0.41 \pm 0.02$	$0.003 \pm 0.0008$	$0.03 \pm 0.008$	$0.08 \pm 0.0009$	$0.003 \pm 0.0005$	$0.002 \pm 0.0005$	$0.005 \pm 0.001$	$0.006 \pm 0.001$



**Fig. 2.** Typical SEM BSE micrographs of the primary  $\text{Al}_3\text{Ti}$  intermetallic compounds from the ingot samples (a) without UST; (b) with UST performed from 810 to 770 °C; (c) with UST performed from 770 to 730 °C; (d) with UST performed from 730 to 690 °C. Note that the scale bars are different in the four figures.

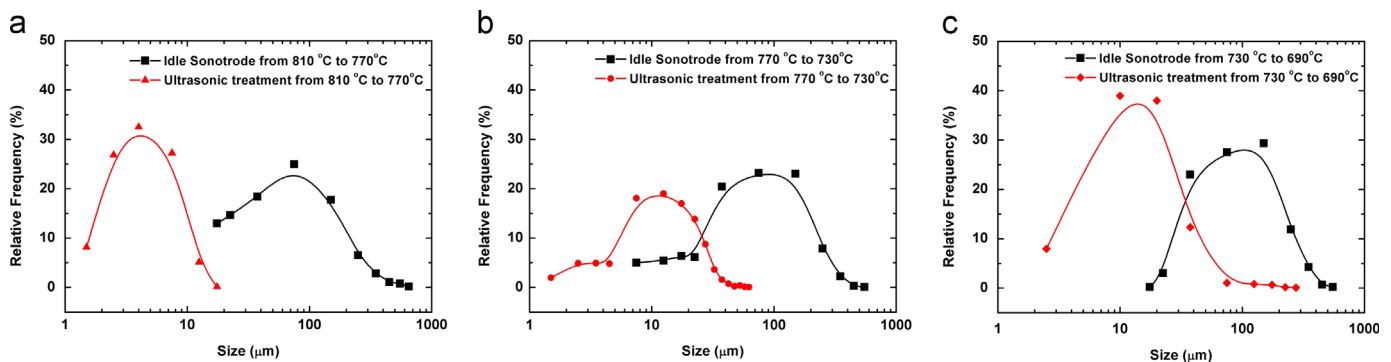


**Fig. 3.** Statistic measurement of the primary  $\text{Al}_3\text{Ti}$  particle size distribution from the ingot samples (a) UST performed from 810 to 770 °C; (b) UST performed from 770 to 730 °C; (c) UST performed from 730 to 690 °C.

distribution of primary particles after the UST from 730 to 690 °C. Although the majority of intermetallics are refined to 10–30  $\mu\text{m}$ , there are still a few particles with the size of > 100  $\mu\text{m}$ , and even larger than 200  $\mu\text{m}$ . The reason for this observation will be discussed in Section 3.3.

### 3.2. Effect of UST on the 3D morphology of primary $\text{Al}_3\text{Ti}$ intermetallic particles

From the SEM micrographs presented in Fig. 4, we can see that the primary  $\text{Al}_3\text{Ti}$  intermetallics in the samples without UST are generally plate-shape phases with their thickness considerably smaller than the other two dimensions. However, Fig. 4(c) and (d) shows that the  $\text{Al}_3\text{Ti}$  particles actually grow in a dendritic manner with four fast-growing crystallographic directions. This agrees well with the well-established theory [15,16] that the intermetallic compounds, which often have higher entropy of fusion due to the greater difference in structure and bonding between the solid and liquid phases, normally have faceted growth morphology. The large growth rate anisotropy of  $\text{Al}_3\text{Ti}$  is related to its crystal structure because different crystallographic planes have different atomic attachment kinetics due to the different planar atom

density.  $\text{Al}_3\text{Ti}$  has a tetragonal crystal structure with the lattice parameters  $a=0.3846$  nm and  $c=0.8594$  nm [17,18]. Based on the Kossel patterns taken at the various positions on the plate surface, previous investigators [19–21] determined that the broad plane of the  $\text{Al}_3\text{Ti}$  plate is {001} plane and all the dendrites grow in the  $\langle 110 \rangle$  directions as indicated in Fig. 4(b) and (d). The reason for the angles between the four crystallographic directions (as indicated in Fig. 4(b) and (d)) being not exactly 90° is that the plates are tilted at various unknown angles to the plane of the micrographs. It is noted that long cracks are observed in some large  $\text{Al}_3\text{Ti}$  plates as highlighted in Fig. 4(b). It is considered that these cracks in combination with the particularly thin plate shape could facilitate the fragmentation of  $\text{Al}_3\text{Ti}$  particles.

Fig. 5 shows the typical morphology of the primary  $\text{Al}_3\text{Ti}$  intermetallics after UST. As we can see, the  $\text{Al}_3\text{Ti}$  particles still have a plate-like morphology but with much smaller size and thickness. We name the refined plate morphology as “tablet”. Moreover, the tablets are still thin relative to other dimensions. Interesting observations of two or three tablets intersecting each other are highlighted in Fig. 5(b) and (d). Three possible mechanisms are proposed: (1) the intersecting tablets are grown from the same nucleus [21,22]; (2) re-entrant twinning occurs during the growth

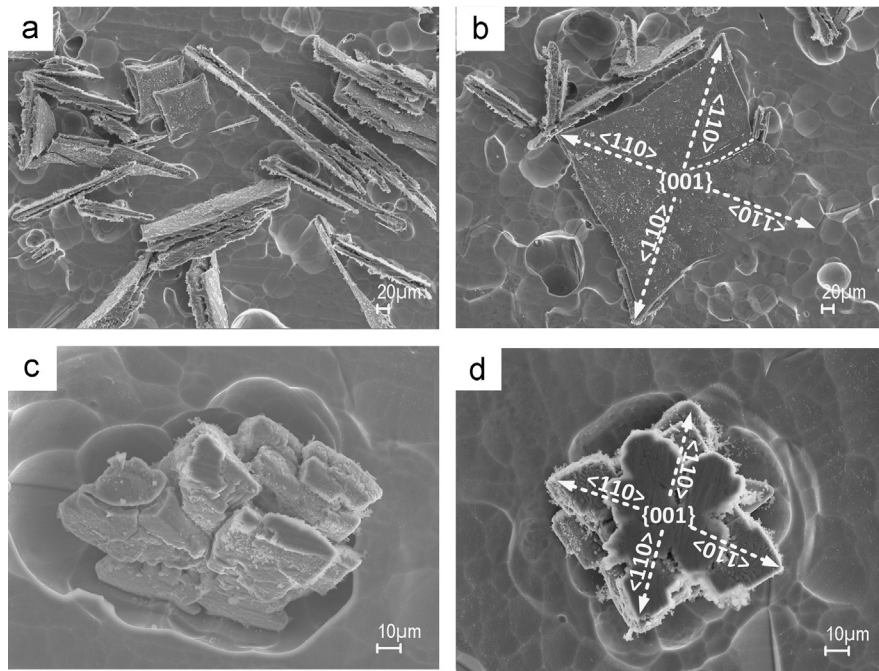


**Fig. 4.** Typical SEM micrographs of the primary  $\text{Al}_3\text{Ti}$  intermetallic compounds in the deeply-etched samples without UST.

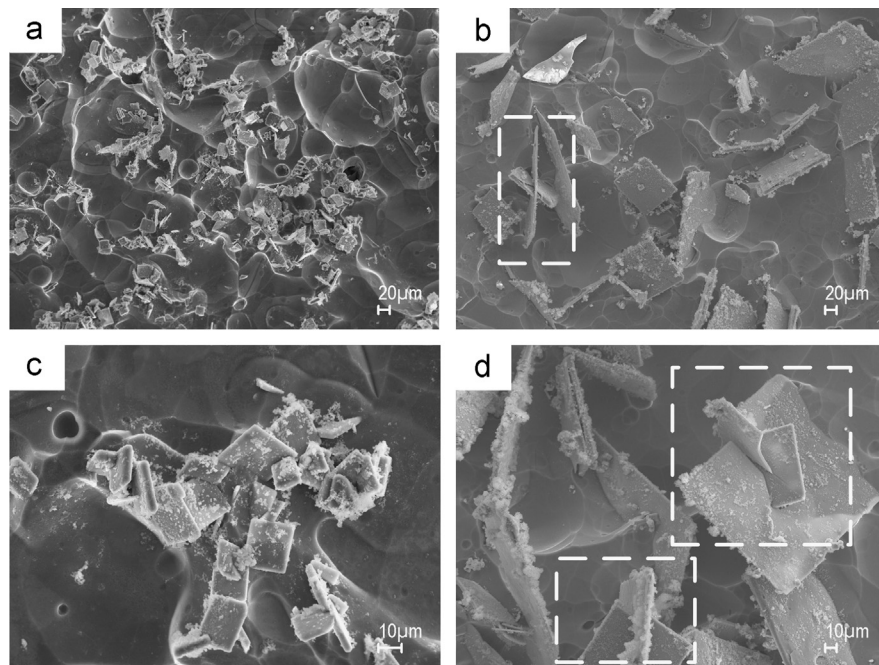


**Fig. 5.** Typical SEM micrographs of the primary  $\text{Al}_3\text{Ti}$  intermetallic compounds in the deeply-etched samples with UST.

of these particles in which both halves of the twin boundary grow rapidly, resulting in the morphology of two intersecting tablets that share a twin relationship; and (3) free-floating intermetallic particles were accelerated as a result of UST streaming and/or cavitation jetting and then collided with each other to form such intersections [23,24].

### 3.3. Mechanisms of UST refinement over the selected temperature ranges

The above results clearly demonstrate that the application of high intensity ultrasound to the Al–0.4Ti alloy over the selected

temperatures has a prominent refinement effect on the primary  $\text{Al}_3\text{Ti}$  intermetallics. However, the precise mechanisms of action of UST over the selected temperature ranges remain unclear. According to the literature, the effects of ultrasonic processing arise from the physical phenomena that occur during the propagation of high intensity ultrasound waves in the liquid. The two most important phenomena [1,2,4,11,12,25] are (i) acoustic cavitation which is the formation, growth and implosive collapse of cavitation bubbles and (ii) acoustic streaming which is the formation of a steady circulation flow driven by acoustic wave propagation and cavitation region pulsation. Based on these phenomena, many hypotheses have been proposed to clarify the

refinement. In general, these hypotheses can be summarised as two theories [1,11,25,26]: (i) the sonocrystallization theory which is based on cavitation-enhanced nucleation and (ii) the sonofragmentation theory which is based on cavitation-induced fragmentation.

The sonocrystallization theory can be further explained by three different mechanisms. The first one [1,27] is based on the idea of activation of substrates by cavitation. Real melt always contains impurity particles such as oxides, carbides, nitrides and borides which often possess crevices and cracks of micron scale on their surface and are non-wettable by the melt due to the presence of a gaseous phase at their surface. It is proposed that the formation, growth and implosive collapse of cavitation bubbles close to the micro-crevices or -cracks produces a high-energy shock-wave or cumulative jet near the impurity particles. Both phenomena would result in the sonocapillary effect which improves the wetting of the impurity particles by the melt and hence activates them to become potent nucleation sites. The second mechanism [28,29] is based on the increased undercooling resulting from an increase of melting point which is caused by the instantaneous pressure spike accompanying the collapse of cavitation bubble according to the Clapeyron equation. The third mechanism [28] suggests that the liquid at the bubble surface cools below the melting temperature and nucleates due to the rapid evaporation of the liquid as the cavitation bubble expands. However, this mechanism seems least probable as the calculation by Hunt and Jackson [28] showed that the temperature drop at the bubble surface is too small to produce nucleation.

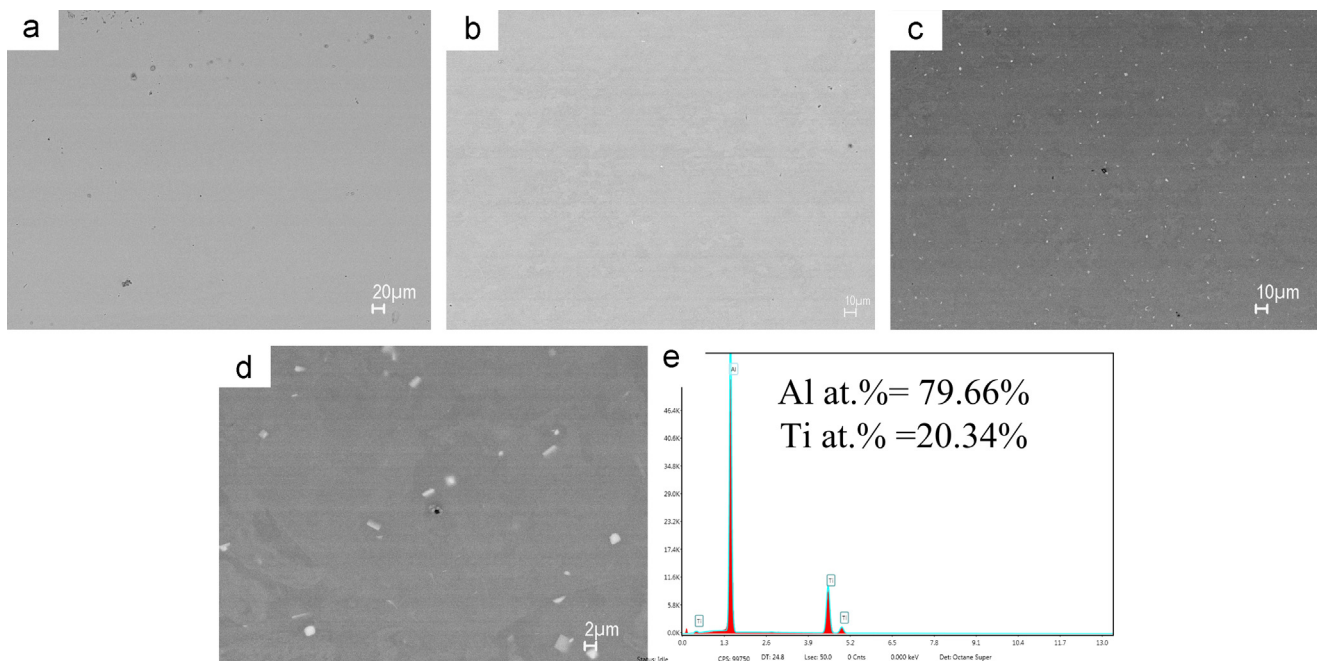
The sonofragmentation theory is based on the assumption that the shockwaves or microjets generated by bubble collapse create shear forces and produce localised erosion on growing solid phase which leads to the breakage of solid phase followed by the solid fragments being distributed throughout the melt via the acoustic streaming [1,2]. It is necessary to note that the sonofragmentation mechanism can only happen when a solid phase already exists in the melt and is present in the cavitation zone.

In order to understand the refinement mechanisms by UST acting over the three selected temperature ranges, the results of

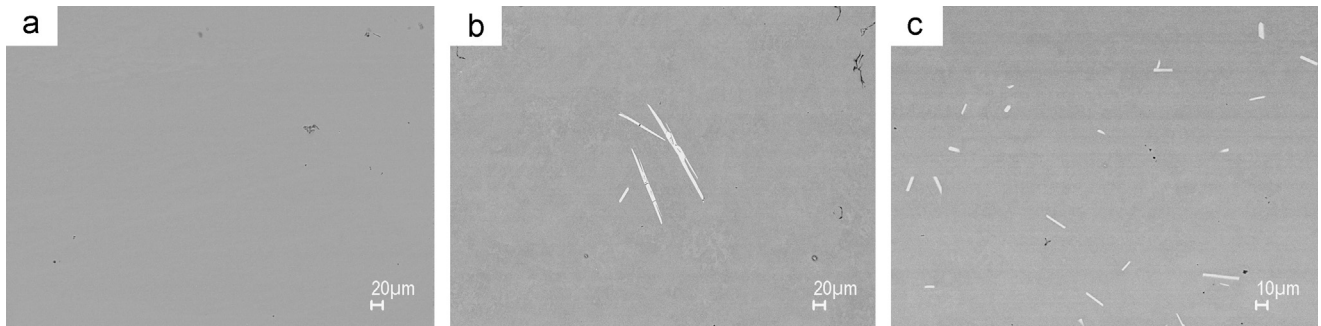
quenching experiments as described in the *Experimental* section are analysed.

Fig. 6 shows the SEM BSE micrographs of the quenched samples, without and with UST from 810 to 770 °C and a corresponding EDS spectrum. As we can see in Fig. 6(a), no particles could be detected when the alloy sample was quenched at 810 °C. This is consistent with the equilibrium phase diagram [30] which shows that there should be no particles but a full liquid at 810 °C as the liquidus temperature of primary  $\text{Al}_3\text{Ti}$  is 768 °C. After the immersion of the idle sonotrode from 810 to 770 °C, the quenched sample at 770 °C as shown in Fig. 6(b) also shows no sign of particles since the quenching temperature is still above the liquidus temperature. This indicates that the cooling rate of the quenching method employed here is sufficiently fast to suppress the nucleation of primary particles during the rapid solidification. However, after UST from 810 to 770 °C, many tiny particles are observed in the quenched sample at 770 °C as presented in Fig. 6(c). The magnified image, Fig. 6(d), clearly shows that they are distinct particles with size around 1–2  $\mu\text{m}$ . The EDS analysis in Fig. 6(e) confirms that these particles are high in Al and Ti with atomic ratio  $\approx 80:20$  which is close to the atomic ratio of  $\text{Al}_3\text{Ti}$  if we take the electron beam size, interaction volume and the particle size into account. As we just discussed, according to the equilibrium phase diagram, no primary particles are expected at a temperature above the liquidus temperature. The observation of primary particles at a quenching temperature above the liquidus temperature after UST can be explained as follows: the nucleation of primary  $\text{Al}_3\text{Ti}$  particles requires relatively smaller undercooling after UST than that without UST and the cooling rate of the quenching method is just not fast enough to suppress this relatively easy nucleation. A comparison with the observation of no particles in the quenched sample at 770 °C without UST suggests that the UST in the fully liquid state from 810 to 770 °C facilitated the pre-nucleation of primary  $\text{Al}_3\text{Ti}$  particles. Since the UST was applied entirely in the liquid state before the nucleation commences, it is most probable that the UST facilitated the nucleation by improving the wetting of indigenous particles present in the melt.

Similarly, the SEM BSE images of the quenched samples without and with UST from 770 to 730 °C are presented in Fig. 7. Again,



**Fig. 6.** SEM BSE micrographs of (a) the quenched sample at 810 °C before inserting sonotrode; (b) the quenched sample at 770 °C without UST but in the presence of idle sonotrode; (c) the quenched sample at 770 °C after UST from 810 °C; (d) the enlarged view of (c); (e) a typical EDS spectrum of the tiny white particles in (c) and (d).



**Fig. 7.** SEM BSE micrographs of (a) the quenched sample at 770 °C before inserting sonotrode; (b) the quenched sample at 730 °C without UST but in the presence of idle sonotrode; (c) the quenched sample at 730 °C after UST from 770 °C.

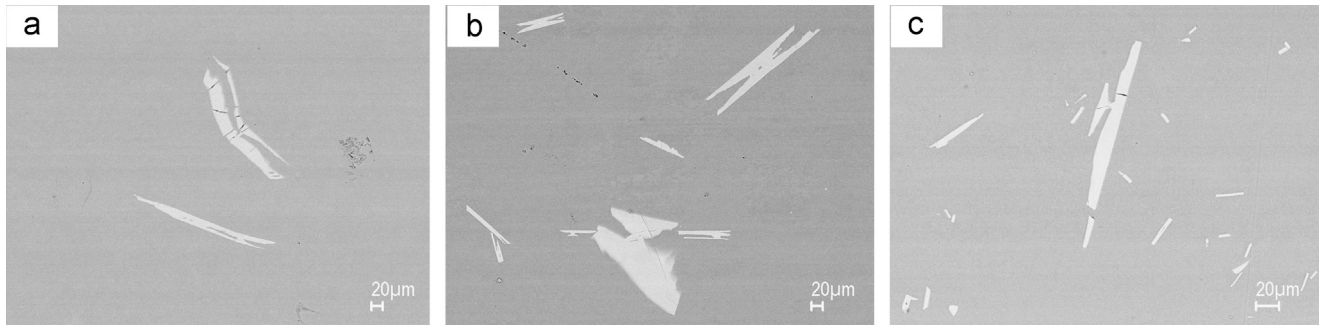


**Fig. 8.** SEM BSE micrographs of (a) the quenched sample at 730 °C before inserting sonotrode; (b) the quenched sample at 690 °C without UST but in the presence of idle sonotrode; (c) the quenched sample at 690 °C after UST from 730 °C.

Fig. 7(a) shows no particles in the quenched sample at 770 °C before inserting the sonotrode. However, large intermetallics are observed in the sample quenched at 730 °C after cooling without UST but in the presence of an idle sonotrode from 770 to 730 °C as shown in Fig. 7(b). This also agrees with the equilibrium phase diagram as 730 °C is below the liquidus temperature and hence primary particles are expected to nucleate and grow. In contrast, the quenched sample at 730 °C after UST from 770 °C shows many smaller intermetallics, indicating that UST has caused refining of the particles. It is also noted that the size distribution is relatively even without particularly larger particles as shown in Figs. 7(c) and 3(b), implying that the cavitation-enhanced nucleation made a major contribution to the refinement, considering the UST started before the onset of nucleation and continued to the growth stage. In addition, the contribution of the fragmentation mechanism cannot be completely ruled out.

Fig. 8 shows the quenched samples without and with UST from 730 to 690 °C. As we can see in Fig. 8(a), the intermetallic particles had grown to a certain size as we could expect from the equilibrium phase diagram when the alloy melt was quenched at 730 °C. Fig. 8(b) shows that the primary particles had further grown to a larger size at 690 °C in the presence of an idle sonotrode without UST. In contrast, with the UST from 730 to 690 °C, the majority of intermetallics had been considerably refined as shown in Fig. 8(c) in which we can also observe a large unrefined particle. A comparison of Fig. 8(a)–(c) clearly suggests that the cavitation-induced fragmentation mechanism dominated the refinement when the UST was performed during the growth stage from 730 to 690 °C.

The presented results clearly show that both sonocrystallization and sonofragmentation mechanisms contribute to the refinement of the primary Al<sub>3</sub>Ti particles observed in the current study. In the fully liquid state such as from 810 to 770 °C, the sonocrystallization mechanism via the activation of native particles as nucleation sites is believed to play the major role in refining the particles while the sonofragmentation mechanism is considered to dominate the refinement effect when the UST is

performed in the growth stage of primary particles. When the application of UST starts before the nucleation commences and terminates at the growth stage, both mechanisms are suggested to work together to refine the primary particles.

#### 4. Conclusions

The refining effect of UST on primary particles was investigated by applying high intensity UST to an Al–0.4Ti alloy over three different temperature ranges which correspond to three different solidification stages: (i) fully liquid state, (ii) across the nucleation stage and (iii) the growth stage. The size and morphology change induced by the UST was studied by SEM. In the light of literature, the mechanisms of refinement observed in the current study were further discussed based on the results of designed quenching experiments. The following conclusions are drawn:

1. Significant refinement of primary particles is produced by UST over all the three selected temperature ranges. This is also accompanied by the morphology change from large dendritic plates to small compact tablets.
2. Cavitation-enhanced nucleation via improved wetting of native particles is suggested to play the dominant role in refinement when the UST is applied in the fully liquid state. Meanwhile, the cavitation-induced fragmentation prevails in the refinement when the UST is carried out in the growth stage.
3. Both mechanisms are believed to contribute to the refinement if the UST starts above the liquidus and continues to the growth stage.

Further in-situ observation and ex-situ characterisation are required to provide direct evidence of the exact mechanisms as regard to how the cavitation enhances the nucleation and how the large primary particles are fragmented in the presence of cavitation.

## Acknowledgements

The authors acknowledge the financial support from UK government's Engineering and Physical Science Research Council (EPSRC) for the Ultra-Cast project (Grant EP/L019884/1, EP/L019825/1, EP/L019965/1).

## References

- [1] G.I. Eskin, D.G. Eskin, *Ultrasonic Treatment of Light Alloy Melts*, CRC Press, Boca Raton, Florida, 2015.
- [2] O.V. Abramov, *High-intensity Ultrasonics: Theory and Industrial Applications*, Gordon and Breach Science Publishers, Amsterdam, The Netherlands, 1998.
- [3] G.I. Eskin, Broad prospects for commercial application of the ultrasonic (cavitation) melt treatment of light alloys, *Ultrason. Sonochem.* 8 (2001) 319–325.
- [4] T.V. Atamanenko, D.G. Eskin, L. Zhang, L. Katgerman, Criteria of grain refinement induced by ultrasonic melt treatment of aluminum alloys containing Zr and Ti, *Metall. Mater. Trans. A* 41 (2010) 2056–2066.
- [5] G.I. Eskin, Cavitation mechanism of ultrasonic melt degassing, *Ultrason. Sonochem.* 2 (1995) S137–S141.
- [6] G.I. Eskin, D.G. Eskin, Production of natural and synthesized aluminum-based composite materials with the aid of ultrasonic (cavitation) treatment of the melt, *Ultrason. Sonochem.* 10 (2003) 297–301.
- [7] G.I. Eskin, D.G. Eskin, Some control mechanisms of spatial solidification in light alloys, *Z. Met.* 95 (2004) 682–690.
- [8] L. Zhang, D.G. Eskin, L. Katgerman, Influence of ultrasonic melt treatment on the formation of primary intermetallics and related grain refinement in aluminum alloys, *J. Mater. Sci.* 46 (2011) 5252–5259.
- [9] F. Wang, Z. Liu, D. Qiu, J.A. Taylor, M.A. Easton, M.X. Zhang, Revisiting the role of peritectics in grain refinement of Al alloys, *Acta Mater.* 61 (2013) 360–370.
- [10] Z. Liu, D. Qiu, F. Wang, J.A. Taylor, M. Zhang, The grain refining mechanism of cast zinc through silver inoculation, *Acta Mater.* 79 (2014) 315–326.
- [11] M. Qian, A. Ramirez, A. Das, Ultrasonic refinement of magnesium by cavitation: Clarifying the role of wall crystals, *J. Cryst. Growth* 311 (2009) 3708–3715.
- [12] A. Ramirez, M. Qian, Grain refinement of magnesium alloys by ultrasonic vibration, in: *TMS 2007 Annual Meeting and Exhibition*, Orlando, FL, 2007, pp. 127–132.
- [13] G. Wang, M.S. Dargusch, M. Qian, D.G. Eskin, D.H. StJohn, The role of ultrasonic treatment in refining the as-cast grain structure during the solidification of an Al–2Cu alloy, *J. Cryst. Growth* 408 (2014) 119–124.
- [14] J.O. Andersson, T. Helander, L. Höglund, P. Shi, B. Sundman, Thermo-Calc & DICTRA, computational tools for materials science, *Calphad* 26 (2002) 273–312.
- [15] J.A. Dantzig, M. Rappaz, *Solidification*, EPFL Press, Lausanne, 2009.
- [16] W. Kurz, D.J. Fisher, *Fundamentals of Solidification*, Trans Tech Publications, Switzerland, 1998.
- [17] J.L.C. Daams, P. Villars, J.H.Nv Vucht, *Atlas of Crystal Structure Types for Intermetallic Phases*, ASM International, Materials Park, Ohio, 1991.
- [18] P. Villars, L.D. Calvert, *Pearson's Handbook of Crystallographic Data for Intermetallic Phases*, ASM International, Materials Park, Ohio, 1991.
- [19] W. Fink, K. Van Horn, P.M. Budge, General-constitution of high-purity aluminum-titanium alloys (with discussion), *AIME Trans.* 93 (1931) 19.
- [20] D.H. John St., L.M. Hogan, Al<sub>3</sub>Ti and the grain refinement of aluminium, *J. Aust. Inst. Met.* 22 (1977) 160–166.
- [21] D.H. John St., L.M. Hogan, Metallography and growth crystallography of Al<sub>3</sub>Ti in Al–Ti alloys up to 5 wt% Ti, *J. Cryst. Growth* 46 (1979) 387–398.
- [22] H. Fredriks, M. Hillert, N. Lange, Modification of aluminum-silicon alloys by sodium, *J. Inst. Met.* 101 (1973) 285–299.
- [23] S.J. Doktycz, K.S. Suslick, Interparticle collisions driven by ultrasound, *Science* 247 (1990) 1067–1069.
- [24] T. Prozorov, R. Prozorov, K.S. Suslick, High velocity interparticle collisions driven by ultrasound, *J. Am. Chem. Soc.* 126 (2004) 13890–13891.
- [25] J.R.G. Sander, B.W. Zeiger, K.S. Suslick, Sonocrystallization and sonofragmentation, *Ultrason. Sonochem.* 21 (2014) 1908–1915.
- [26] T.V. Atamanenko, D.G. Eskin, M. Sluiter, L. Katgerman, On the mechanism of grain refinement in Al–Zr–Ti alloys, *J. Alloy. Compd.* 509 (2011) 57–60.
- [27] Y. Han, K. Li, J. Wang, D. Shu, B. Sun, Influence of high-intensity ultrasound on grain refining performance of Al–5Ti–1B master alloy on aluminium, *Mater. Sci. Eng. A* 405 (2005) 306–312.
- [28] J.D. Hunt, K.A. Jackson, Nucleation of solid in an undercooled liquid by cavitation, *J. Appl. Phys.* 37 (1966) 254–257.
- [29] J.D. Hunt, K.A. Jackson, Nucleation of the solid phase by cavitation in an undercooled liquid which expands on freezing, *Nature* 211 (1966) 1080–1081.
- [30] I. Ohnuma, Y. Fujita, H. Mitsui, K. Ishikawa, R. Kainuma, K. Ishida, Phase equilibria in the Ti–Al binary system, *Acta Mater.* 48 (2000) 3113–3123.